

First-order structural transition in the magnetically ordered phase of $\text{Fe}_{1.13}\text{Te}$

S. Rößler,^{1,*} Dona Cherian,² W. Lorenz,³ M. Doerr,³ C. Koz,¹ C. Curfs,⁴
Yu. Prots,¹ U. K. Rößler,⁵ U. Schwarz,¹ Suja Elizabeth,² and S. Wirth¹

¹Max Planck Institute for Chemical Physics of Solids, Nöthnitzer Straße 40, 01187 Dresden, Germany

²Department of Physics, C.V. Raman Avenue, Indian Institute of Science, Bangalore-560012, India

³Institut für Festkörperphysik, Technische Universität Dresden, 01062 Dresden, Germany

⁴ESRF, 6 Rue Jules Horowitz, BP 220, 38043 Grenoble Cedex 9, France

⁵IFW Dresden, Postfach 270016, 01171 Dresden, Germany

(Dated: February 21, 2022)

Specific heat, resistivity, magnetic susceptibility, linear thermal expansion (LTE), and high-resolution synchrotron X-ray powder diffraction investigations of single crystals Fe_{1+y}Te ($0.06 \leq y \leq 0.15$) reveal a splitting of a single, first-order transition for $y \leq 0.11$ into two transitions for $y \geq 0.13$. Most strikingly, all measurements on identical samples $\text{Fe}_{1.13}\text{Te}$ consistently indicate that, upon cooling, the magnetic transition at T_N precedes the first-order structural transition at a lower temperature T_s . The structural transition in turn coincides with a change in the character of the magnetic structure. The LTE measurements along the crystallographic c -axis displays a small distortion close to T_N due to a lattice striction as a consequence of magnetic ordering, and a much larger change at T_s . The lattice symmetry changes, however, only below T_s as indicated by powder X-ray diffraction. This behavior is in stark contrast to the sequence in which the phase transitions occur in Fe pnictides.

PACS numbers: 74.70.Xa, 65.40.De, 65.60.+a

I. INTRODUCTION

The recent discovery¹ of superconductivity in iron-based $\text{LaFeAsO}_{1-x}\text{F}_x$ (a member of the so-called 1111 family) with a transition temperature $T_c = 26$ K ignited tremendous experimental and theoretical interest surrounding this family of compounds. The superconducting members of the ferropnictides exhibit transition temperatures as high as 56 K.² These materials display a strong competition between structural, magnetic, and superconducting transitions. One of the features common to both the high- T_c copper oxide and Fe-based superconductors is that the superconductivity emerges when an antiferromagnetic order is suppressed by chemical substitution or doping. While the initial interest was driven by the discovery of superconductivity in different crystal systems with higher T_c , the current emphasis is focused on understanding the origin of the magnetic order and its relation to the superconductivity. The members of the 1111 family undergo a structural transition (T_s) followed by a magnetic transition (T_N) at lower temperatures,³⁻⁶ whereas in the 122 compounds these two transitions occur simultaneously.⁷⁻⁹ Several theoretical models have been proposed for the possible microscopic mechanisms coupling the magnetic and structural transitions. Among these, the prominent ones are the itinerant-electron model based on the nesting properties of the Fermi surface,¹⁰ the local moment J_1J_2 model favoring a spin-nematic-driven structural transition,^{11,12} and an implementation of orbital ordering into the double exchange model¹³ where the structural transition is induced by an orbital, rather than a magnetic, ordering. On the other hand, a phenomenological Ginzburg-Landau model shows that the magneto-elastic

coupling between the different order parameters can explain some of the experimentally observed phase transition scenarios.¹⁴ However, none of the theories developed up to now predict a possibility of a structural transition taking place well within the magnetically ordered phase, *i.e.* for magnetic ordering occurring at a higher temperature than the structural transition, $T_N > T_s$, in Fe pnictides and chalcogenides.

Tetragonal Fe_{1+y}Te , the non-superconducting phase, occurs only with excess iron in the range $0.06 \leq y \leq 0.15$. Its crystal structure is intermediate between the PbO ($B10$) and Cu_2Sb ($C38$) types. It may be regarded as either PbO type with less than 0.2 extra atoms per cell, or Cu_2Sb with more than 0.8 unoccupied Fe sites,¹⁵ both described within the $P4/nmm$ space group. The nature of the antiferromagnetism in this material is remarkably different in comparison to the FeAs superconductors. In the FeAs based systems, the propagation vector of the spin-density-wave (SDW) is (π, π) with respect to the tetragonal lattice. This corresponds to a wave vector connecting the Γ and M points in the Brillouin zone. In Fe_{1+y}Te , in contrast, the corresponding wave vector is $(\pi, 0)$, *i.e.* it is rotated by 45° with respect to the ordering in the FeAs families.¹⁶⁻¹⁸ This implies that in Fe_{1+y}Te the nesting properties of the Fermi surface do not play any role in the origin of the antiferromagnetism. However, up to now it has been believed that, in similarity to the 122 family, the antiferromagnetic transition at around $T_N = 68$ K is simultaneously accompanied by a first-order structural distortion to the monoclinic space group $P2_1/m$.¹⁷ With increasing amount of interstitial Fe the wave vector changes to an incommensurate $(\delta\pi, 0)$, and the crystal structure adopts a higher symmetry (orthorhombic space group $Pmnm$) at low temperatures.¹⁶

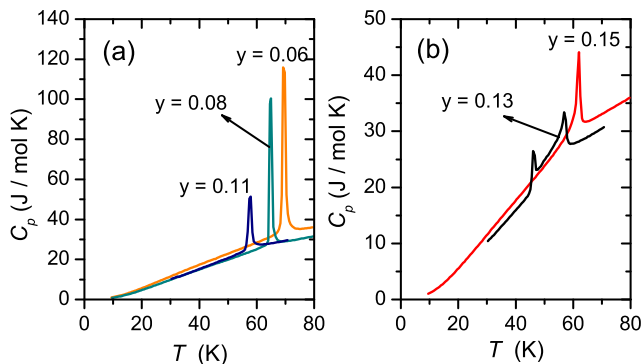


FIG. 1: Specific heat $C_p(T)$ of Fe_{1+y}Te for (a) $y = 0.06, 0.08, 0.11$, and (b) $y = 0.13$ and 0.15 .

Moreover, a very recent neutron scattering experiment¹⁹ revealed that the magnetic structure in Fe_{1+y}Te is even more complex: at a critical concentration $y = 0.124$, the magnetic structure turns into an incommensurate helix.

Here, we report on concerted investigations on Fe_{1+y}Te with $0.06 \leq y \leq 0.15$, with focus on samples with $y = 0.11$ and 0.13 , *i.e.* around the critical concentration. It is found that the T_N decreases systematically from 70 K for $y = 0.06$ to 57 K for $y = 0.11$. Most importantly, we demonstrate that the magnetic and structural transitions in $\text{Fe}_{1.13}\text{Te}$ are separated in temperature by about 11 K, with the antiferromagnetic ordering occurring at higher temperature than the structural transition. Our results show that the magnetic behavior in the pnictides and chalcogenides could be entirely different and cast a serious challenge to many existing theories of Fe superconductors.

II. EXPERIMENTAL DETAILS

Single crystals Fe_{1+y}Te were grown using a horizontal Bridgman setup. The details of the crystal growth procedure were similar to those described in Ref. [20], except for a different cooling rate. In the present case of Fe_{1+y}Te , after furnace translation, the samples were cooled down at a rate of 5 °C/h from 950 °C to 700 °C, followed by cooling to room temperature with 25 °C/h. The crystals were characterized by Laue photographs, powder X-ray diffraction, chemical analysis, and EDXS. The composition y was determined from the lattice parameters²¹ calibrated for mass loss during growth, and EDXS. The specific heat $C_p(T)$ was measured using a Quantum Design physical property measurement system (PPMS) with a heat-pulse relaxation technique. At each measured temperature data point, 2 % temperature rise and a measurement time with two time constants were used. The electrical resistivity $\rho(T)$ was also measured using the PPMS whereas the magnetic susceptibility $\chi(T)$ was obtained by means of a SQUID vibration sample magnetometer. The diffraction data were col-

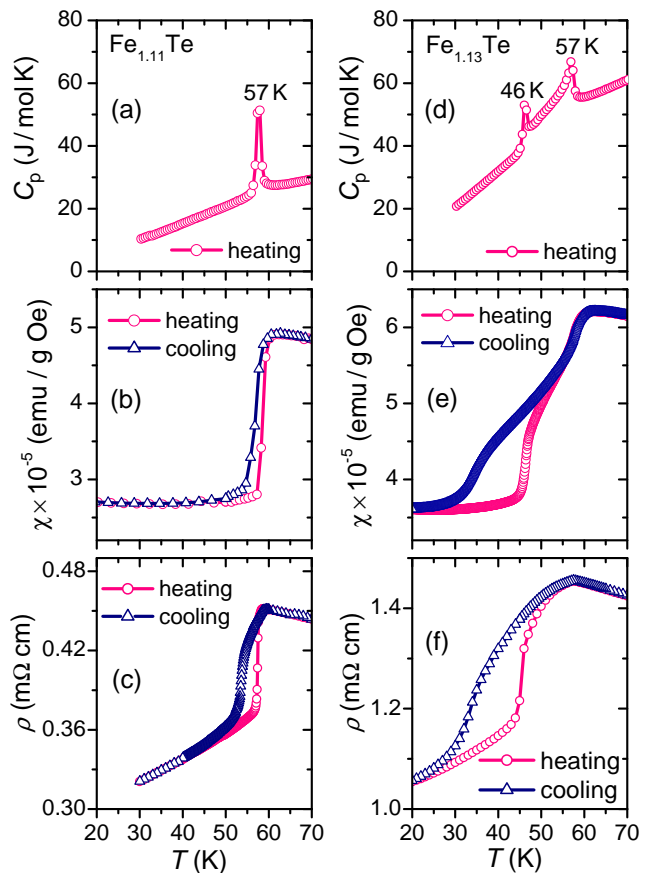


FIG. 2: Specific heat, dc magnetic susceptibility, and resistivity (from top to bottom) of $\text{Fe}_{1.11}\text{Te}$ (left) and $\text{Fe}_{1.13}\text{Te}$ (right) single crystals. The magnetic susceptibility was measured in a field of 0.1 T applied along the ab -plane.

lected on the high-resolution powder diffraction beamline ID31 (wavelength of 39.992 pm) at the ESRF, Grenoble, using a liquid-He cryostat. A sensitive tilted-plate capacitive dilatometer²² with a resolution of relative length changes $\Delta l/l_0 = 10^{-7}$ was employed to measure the linear thermal expansion (LTE) along the crystallographic c axis.

III. RESULTS AND DISCUSSION

The temperature dependence of specific heat $C_p(T)$ of Fe_{1+y}Te for $y = 0.06, 0.08, 0.11, 0.13$, and 0.15 is presented in Fig. 1. For $y = 0.06$, C_p shows a sharp first-order peak corresponding to a simultaneous magnetic and structural transition at $T_N = T_s \sim 70$ K. This transition temperature monotonically decreases to 57 K with y increasing to 0.11. The transition temperature is drastically suppressed with respect to that in $\text{Fe}_{1.06}\text{Te}$ due to the increased amount of interstitial Fe, a finding consistent with previous studies.²³ Instead of a continued suppression of T_N , the further increased amount of interstitial Fe in $\text{Fe}_{1.13}\text{Te}$ gives rise to a dramatically

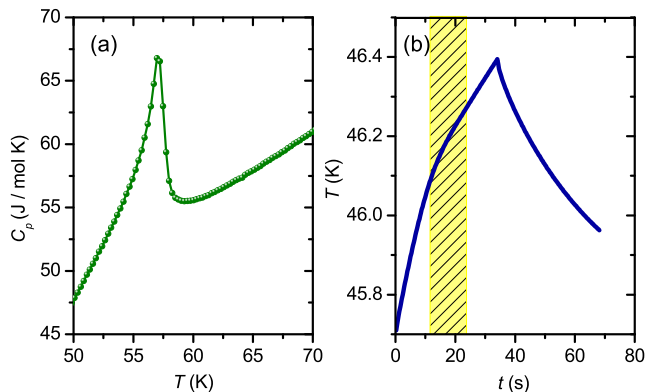


FIG. 3: (a) High temperature-resolution specific heat data for $\text{Fe}_{1.13}\text{Te}$ showing a clear λ -like transition at 57 K. (b) The temperature-time relaxation curve depicting the arrests (shaded region) due to latent heat at the first-order phase transition at $T \sim 46$ K in $\text{Fe}_{1.13}\text{Te}$.

different behavior, Fig. 1(b). Two clearly distinct transitions are observed: First, a λ -like transition at 57 K, followed by a first-order phase transition at 46 K. For even more interstitial Fe, $y = 0.15$, the temperature at which the λ -like transition occurs increases to 63 K, but the low-temperature first-order transition could not be clearly resolved in the specific heat measurements.

To investigate the nature of phase transitions in Fe_{1+y}Te around the critical concentration where successive phase transitions occur, we conducted magnetic susceptibility $\chi(T)$ and electrical resistivity $\rho(T)$ measurements for $y = 0.11$ and 0.13 . In Fig. 2, $\chi(T)$ and $\rho(T)$ data are presented along with $C_p(T)$ for these samples for comparison. $C_p(T)$ in Fig. 2(a) clearly displays a sharp first-order transition at 57 K. This temperature corresponds to a simultaneous structural and SDW transition, $T_s \approx T_N$. The coincident SDW transition is confirmed by a sudden decline in the magnetic susceptibility $\chi(T)$ around 57 K, Fig. 2(b). The cooling and heating susceptibility cycles measured in a field of 0.1 T show a thermal hysteresis typical for a first-order phase transition. The in-plane (ab plane) resistivity $\rho(T)$ displays a corresponding transition from a semiconducting to metallic behavior, as can be seen in Fig. 2(c). In Fig. 2(d), $C_p(T)$ for $\text{Fe}_{1.13}\text{Te}$ is given. The high-temperature transition at $T_N = 57$ K in Fig. 2(d) is unmistakable λ -like, proving that the phase transition is of second order, and can be described by a power law divergence. The λ -like shape of this transition is obvious in the high temperature-resolution data provided in Fig. 3(a). The transition at lower temperature, $T_s = 46$ K, in $\text{Fe}_{1.13}\text{Te}$ is similar in shape to the single one observed in $\text{Fe}_{1.11}\text{Te}$ (see Fig. 2(a)), where a latent heat is involved and hence, is of first-order in nature. In order to confirm the first-order nature of the transition, the temperature-time relaxation curve is presented in Fig. 3(b). It clearly displays a temperature arrest around 46 K in the warming part (shaded region) of the relaxation curve. As expected for this case,

it clearly displays a first-order nature of the transition. In the cooling part, however, the temperature arrest was not observed, suggesting that the first-order transition is spread over a wider temperature interval. This argument is also supported by a broader transition observed in the $\chi(T)$ cooling measurement, Fig. 2(e). This finding, along with the results presented below, indicates that a change in the crystal structure occurs only at the low-temperature transition. With this assignment the lower values of C_p just below T_s suggest a discontinuous jump in the phononic background. This typically happens at a structural transition due to softened optical phonons.

A continuous transition followed by a first-order transition in $\text{Fe}_{1.13}\text{Te}$ can also be discerned from the susceptibility measurements shown in Fig. 2(e): $\chi(T)$ first decreases continuously at around 57 K, followed by a sharp jump upon further reduction of temperature. A huge thermal hysteresis covering a width of ≈ 25 K in the field-cooled and heating protocols was found only at the low temperature transition. However, the thermal hysteresis in the resistivity is broader and remains up to the high temperature transition, Fig. 2(f). Here we note that similar successive phase transitions have also been observed in resistivity measurements on $\text{Fe}_{1.086}\text{Te}$ above an applied pressure of about 1 GPa.²⁴ This suggests that the addition of interstitial Fe beyond $y > 0.11$ produces similar effects like application of pressure on Fe_{1+y}Te with smaller amount y of interstitial Fe.

In order to unambiguously confirm the above assignment of the structural transition to $T_s = 46$ K in $\text{Fe}_{1.13}\text{Te}$ we performed high-resolution synchrotron X-ray diffraction of the powdered single crystals at several selected temperatures. In Fig. 4, the diffraction data collected above T_N (300 K, 64 K), between T_N and T_s (52 K), and below T_s (40 K) are presented. The pattern at 300 K could be well fitted within the tetragonal $P4/nmm$ space group,^{16,17} see Fig. 4(b). Upon crossing $T_N = 57$ K, the structure remains unchanged, *i.e.* tetragonal, as can be seen from the pattern at $T = 52$ K. Note that at 52 K, the peak corresponding to the (200) reflection starts to broaden indicating a structural instability arising due to the fluctuations in the vicinity of the phase transition. Notably, the pattern at 40 K is clearly different. The observed splitting of the diffraction peaks, specifically of the tetragonal (200) at higher T into (200) and (020) at 40 K [see Fig. 4(a)], is compatible with an orthorhombic symmetry below T_s . Moreover, the intensities observed at 40 K can be described by a structure model in the space group $Pm\bar{m}n$. This result is consistent with neutron scattering studies on $\text{Fe}_{1.141}\text{Te}$.¹⁶

In Fig. 5(a) and (b), we present the LTE $\Delta l/l_0$ and the corresponding LTE coefficient $\alpha(T) = (1/l_0)(dl/dT)$ of the $\text{Fe}_{1.13}\text{Te}$ sample along the crystallographic c axis. Upon cooling, the LTE first displays a shoulder at $T \sim 62$ K due to the incommensurate antiferromagnetic order, followed by a broadened jump at the structural transition. A discontinuity corresponding to the latter transition is nicely resolved in $\alpha(T)$ at $T \approx 41$ K, Fig. 5(b). The

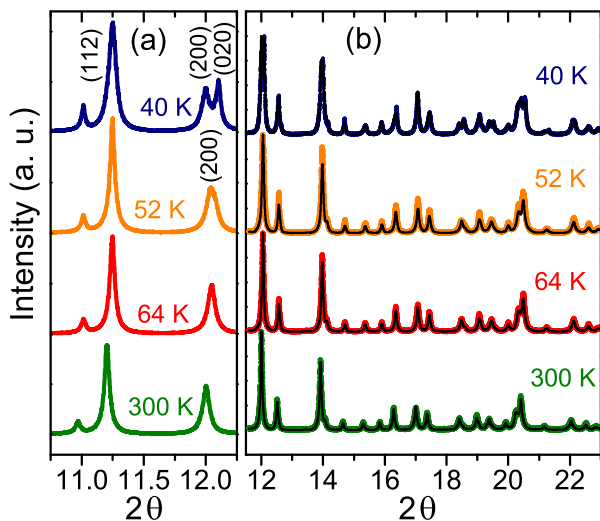


FIG. 4: Synchrotron X-ray diffraction of the powdered $\text{Fe}_{1.13}\text{Te}$ single crystal at temperatures above $T_N = 57$ K, between T_N and T_s , and below $T_s = 46$ K, respectively. (a) Zoomed range $10.75^\circ \leq 2\theta \leq 12.25^\circ$. The single (112) peak and the splitting of the (200) tetragonal peak into two peaks (200) and (020) at $T = 40$ K $< T_s$ indicate an orthorhombic low-temperature structure. (b) Overview spectra $11.5^\circ \leq 2\theta \leq 23^\circ$. The black lines represent fitted curves.

LTE curve very much resembles the one for $\chi(T)$ upon cooling in Fig. 2(e). For increasing temperature, $\Delta l/l_0$ displays a large thermal hysteresis and a sharp increase at $T \approx 46$ K due to the structural transition. However, the transition corresponding to the magnetic ordering in the warming cycle occurs at around 57 K, *i.e.* at a significantly lower temperature than the corresponding transition in the cooling cycle. This kind of reverse hysteresis is rather unusual for a continuous phase transition (see discussion below).

Combining our results with those from neutron scattering experiments^{16,19} allows a detailed interpretation of the magnetic and structural transitions in Fe_{1+y}Te . For low Fe concentrations within the range $0.06 < y < 0.11$, the structural transition assigned to the monoclinic $P2_1/m$ space group appears to take place simultaneously with magnetic ordering as a first-order magneto-elastic transition, as depicted in the schematic phase diagram Fig. 6. For $\text{Fe}_{1.124}\text{Te}$, an incommensurate helix is found with a propagation vector $(q, 0, \frac{1}{2})$ r. l. u. where $q \sim 0.445$, which decreases to 0.4 with increasing temperature in an intermediate range 40 K $< T < 57$ K.¹⁹ Within the same temperature range, this helicoid and an incommensurate SDW with different period $q \sim 0.38$ are observed simultaneously.¹⁹ This is assigned as a complex magnetic phase in Fig. 6. Symmetry considerations strongly restrict the possible phase transition mechanism for the formation of the helimagnetic state. The paramagnetic space group $P4/nmm$ comprises only one-dimensional irreducible representations in the little group for propagation vectors $(q, 0, \frac{1}{2})$.^{25,26} Thus, a continuous transition

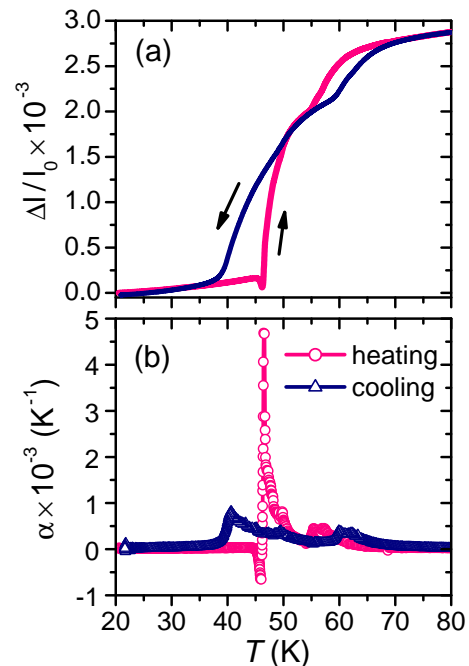


FIG. 5: (a) The linear thermal expansion (LTE) of the $\text{Fe}_{1.13}\text{Te}$ single crystal measured along the crystallographic c axis in both cooling and heating cycles. (b) The corresponding coefficients of the LTE, $\alpha(T) = (1/l_0)(dl/dT)$.

from the paramagnetic into the helical state cannot take place as a mode instability according to standard Landau theory.²⁷ However, there are Lifshitz-type invariants that couple different irreducible representations and can (i) produce a helimagnetic state and (ii) give rise to the nucleation of kink-like modulations of the basic helical modulation on a mesoscopic length scale.²⁶⁻²⁹ The existence of Lifshitz-invariants in helimagnets with strong phase-amplitude interaction causes unconventional magnetic ordering transitions³⁰. Anisotropic magnetic couplings can cause continuous or discontinuous transitions.²⁹ The presence of such anisotropies in Fe_{1+y}Te is suggested by the lock-in transition at $y < 0.11$ and the marked magnetostructural transition in this composition range. Turner *et al.* have proposed a model with localized Fe moment coupled to an orbital order,¹³ which could provide a microscopic mechanism for the magneto-elastic coupling that should vary with y in Fe_{1+y}Te . Thus, for $y > 0.11$ a similar locking-in of the helix may occur owing to possible anisotropic couplings. But, this lock-in transition produces an incommensurate magnetic ordering. This can be understood phenomenologically, if the free energy of the structural order parameter contains dispersive couplings.²⁶ Owing to the intrinsic disorder by the partially occupied Fe sublattice, strong pinning of the kink-like solitons, *i.e.* domain walls between regions with SDW and helical order, will occur. The very wide hysteresis in our LTE data is consistent with such a pinning. Thus, we explain our results in $\text{Fe}_{1.13}\text{Te}$ by a magnetostructural transformation of the helix in the tetragonal

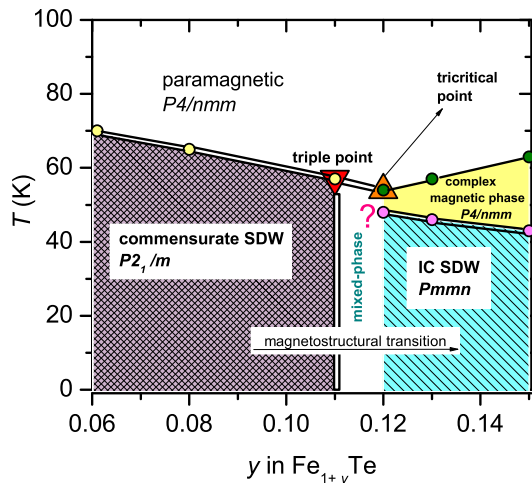


FIG. 6: A tentative schematic temperature-composition phase diagram of Fe_{1+y}Te based on our specific heat, LTE, and X-ray diffraction results (circles, color online) as well as on results of Refs.^{16,19}. The double lines depict a first-order phase transition, the single line represents a continuous phase transition. The origin of the low-temperature first-order line is unclear, therefore marked by “?”. IC SDW denotes an incommensurate spin-density wave.

lattice state into a SDW with orthorhombic distortions subject to strong pinning. This is also in line with the observation of co-existing SDW and helicoidal order associated with different lattice structures in $\text{Fe}_{1.124}\text{Te}$, which was detected by diffraction in neutron scattering experiments.¹⁹ The transformation process can be pictured as a decomposition of the magnetic helix into an incoherent sequence of SDW sections with interspersed helicoidal kinks on a *mesoscopic length scale*.

Features of two successive phase transition have been earlier observed by Hu *et al.*³¹ in $\text{Fe}_{1.09}\text{Te}$ and $\text{Fe}_{1.14}\text{Te}$. However, they did not associate these transitions to individual magnetic and structural phase transitions. Instead, their results were explained based on the nesting properties of the Fermi surface: the higher level of excess Fe corresponds to larger size mismatch between cylindrical electron and hole Fermi surfaces. The two transitions may then represent successive SDW Fermi-surface nestings of separate electron-hole cylindrical pieces. However, neutron scattering studies¹⁶ indicated that the Fermi surface nesting does not play a role in the magnetic ordering in Fe_{1+y}Te . More recently, Zaliznyak *et al.*³² report $\chi(T)$ data for $\text{Fe}_{1.09}\text{Te}$ which is very similar to those of our sample $\text{Fe}_{1.13}\text{Te}$. From the neutron scattering studies on $\text{Fe}_{1.1}\text{Te}$, Zaliznyak *et al.* first find a structural distortion at $T_s = 63$ K, followed by a magnetic ordering at $T_N = 57.5(5)$ K. At $T_m \leq 45$ K, a lock-in transition was observed at an incommensurate wave-vector $(0.48, 0, \frac{1}{2})$. The (201) lattice Bragg peak in their studies does not show a clear splitting down to 9 K. From their data,³² it was not possible to distinguish between the monoclinic $P2_1/m$ and the orthorhombic $Pnmm$ structures. Since

no phase transition features were observed either in the susceptibility or in the specific heat at 63 K, the structural distortion at $T_s = 63$ K was identified from the onset of broadening of (201) reflection. But, such a broadening may also be associated with a symmetry-preserving lattice striction caused by a strong magneto-elastic coupling close to T_N . This distortion is followed by a change in the crystal symmetry at the first-order lock-in transition at 45 K, as observed in our high resolution diffraction data. Thus, we propose that the structural transition occurs simultaneously at a temperature where a change in the character of magnetic structure also takes place well within the magnetically ordered phase.

The symmetry changing structural phase-transition in the magnetically ordered phase is unusual in the parent compounds of Fe-superconductors. In the case of 1111 pnictides³⁻⁶ or partially Co substituted BaFe_2As_2 ^{33,34} and CaFe_2As_2 ,³⁵ where these two phase transitions occur separately, the structural transition always takes place at a higher temperature than T_N . Within an effective Heisenberg-type local-moment (J_1 - J_2 - J_z) model, this splitting arises as a consequence of Ising-like magnetic couplings^{12,36,37} with a very weak interlayer interaction. In support of this theory, the temperature gap between T_s and T_N was experimentally found to increase with increasing distance between FeAs layers.⁵ In the case of Fe_{1+y}Te , however, the c -lattice constant decreases with increasing y .^{16,21} Yet the successive phase transitions occur for $y \geq 0.12$; *i.e.*, for the compositions with shorter c -lattice constant. Thus, the microscopic mechanisms driving the phase transitions in Fe_{1+y}Te seems to be fundamentally different from those in the case of Fe-arsenides.

IV. CONCLUSIONS

In conclusion, our thermodynamic, structural, and thermal expansion data on $\text{Fe}_{1.13}\text{Te}$ give clear evidence for magnetic ordering taking place at *higher* temperatures than the structural phase transition. The structural transition in turn coincides with a change in the nature of the magnetic structure. This is exactly opposite to the behavior observed in the 1111-systems, for which the magnetic transition occurs at lower temperatures than the structural one. The exact nature of the microscopic coupling mechanisms in Fe_{1+y}Te needs to be explored further as it appears to be key in understanding the interplay between localized and itinerant magnetism as well as superconductivity in Fe chalcogenides. As the pairing mechanism in both cuprates and Fe-superconductors probably involves spin fluctuations, understanding the nature of magnetic interactions is of utmost importance.

V. ACKNOWLEDGEMENTS

We thank C. Geibel, Yu. Grin, Q. Si, F. Steglich, O. Stockert, P. Thalmeier, and L. H. Tjeng for stimu-

lating discussions. This work is partially supported by DAAD - DST exchange program ID 50726385.

-
- * Electronic address: roessler@cpfs.mpg.de
- ¹ Y. Kamihara, T. Watanabe, M. Hirano, and H. Hosono, *J. Am. Chem. Soc.* **130**, 3296 (2008).
 - ² C. Wang *et al.*, *Europhys. Lett.* **83**, 67006 (2008).
 - ³ C. de La Cruz *et al.*, *Nature (London)* **453**, 899 (2008).
 - ⁴ H.-H. Klauss *et al.*, *Phys. Rev. Lett.* **101**, 077005 (2008).
 - ⁵ Y. Luo *et al.*, *Phys. Rev. B* **80**, 224511 (2009).
 - ⁶ A. Jesche, C. Krellner, M. de Souza, M. Lang, and C. Geibel, *Phys. Rev. B* **81**, 134525 (2010).
 - ⁷ M. Rotter, M. Tegel, D. Johrendt, I. Schellenberg, W. Hermes, R. Pöttgen, *Phys. Rev. B* **78**, 020503 (2008).
 - ⁸ A. Jesche *et al.*, *Phys. Rev. B* **78**, 180504 (2008).
 - ⁹ N. Ni, S. Nandi, A. Kreyssig, A. I. Goldman, E. D. Mun, S. L. Bud'ko, P. C. Canfield, *Phys. Rev. B* **78**, 014523 (2008).
 - ¹⁰ V. Barzykin and L. P. Gor'kov, *Phys. Rev. B* **79**, 134510 (2009).
 - ¹¹ C. Fang, H. Yao, W. F. Tsai, J. P. Hu, and S. A. Kivelson, *Phys. Rev. B* **77**, 224509 (2008).
 - ¹² C. Xu, M. Müller, and S. Sachdev, *Phys. Rev. B* **78**, 020501 (2008).
 - ¹³ A. M. Turner, F. Wang, and A. Vishwanath, *Phys. Rev. B* **80**, 224504 (2009).
 - ¹⁴ A. Cano, M. Civelli, I. Eremin, and I. Paul, *Phys. Rev. B* **82**, 020408 (2010).
 - ¹⁵ H. Okamoto and L. E. Tanner, *J. Phase Equilib.* **11**, 371 (1990).
 - ¹⁶ W. Bao *et al.*, *Phys. Rev. Lett.* **102**, 247001 (2009).
 - ¹⁷ S. Li *et al.*, *Phys. Rev. B* **79**, 054503 (2009).
 - ¹⁸ T. J. Liu *et al.*, *Nature Mater.* **9**, 718 (2010).
 - ¹⁹ E. E. Rodriguez, C. Stock, P. Zajdel, K. L. Krycka, C. F. Majkrzak, P. Zavalij, M. A. Green, *Phys. Rev. B* **84**, 064403 (2011).
 - ²⁰ S. Röbner, D. Cherian, and S. Harikrishnan, H. L. Bhat, S. Elizabeth, J. A. Mydosh, L. H. Tjeng, F. Steglich, S. Wirth, *Phys. Rev. B* **82**, 144523 (2010).
 - ²¹ C. Koz, U. Schwarz, Yu. Grin *et al.*, to be published.
 - ²² M. Rotter, H. Müller, E. Gratz, M. Doerr, and M. Loewenhaupt, *Rev. Sci. Instrum.* **69**, 2742 (1998).
 - ²³ T. J. Liu *et al.*, *Phys. Rev. B* **80**, 174509 (2009).
 - ²⁴ H. Okada, H. Takahashi, Y. Mizuguchi, Y. Takano, and H. Takahashi, *J. Phys. Soc. Jpn.* **78**, 083709 (2009).
 - ²⁵ C. J. Bradley and B. L. Davis, *Rev. Mod. Phys.* **40**, 359 (1968).
 - ²⁶ J. C. Tolédano and P. Tolédano, *The Landau theory of phase transitions* (World Scientific, 1987).
 - ²⁷ P. G. de Gennes, *Fluctuations Instabilities and Phase transitions*, vol. 2 of NATO ASI Ser. B, ed. T. Riste (Plenum, New York, 1975).
 - ²⁸ I. E. Dzyaloshinskii, *Sov. Phys. JETP* **19**, 960 (1964).
 - ²⁹ B. Schaub and D. Mukamel, *Phys. Rev. B* **32**, 6385 (1985).
 - ³⁰ U. K. Röbner, A. A. Leonov, and A. N. Bogdanov, submitted to PRB (2011).
 - ³¹ R. Hu, E. S. Bozin, J. B. Warren, and C. Petrovic, *Phys. Rev. B* **80**, 214514 (2009).
 - ³² I. A. Zaliznyak, Z. J. Xu, J. Wen, J. M. Tranquada, G. D. Gu, V. Solovyov, V. N. Glazkov, A. I. Zheludev, V. O. Garlea, and M. B. Stone, arXiv:1108.5968 (2011).
 - ³³ J. -H. Chu, J. G. Analytis, C. Kucharczyk, and I. R. Fisher, *Phys. Rev. B* **79**, 014506 (2009).
 - ³⁴ D. K. Pratt, W. Tian, A. Kreyssig, J. L. Zarestky, S. Nandi, N. Ni, S. L. Bud'ko, P. C. Canfield, A. I. Goldman, and R. J. McQueeney, *Phys. Rev. Lett.* **103**, 087001 (2009).
 - ³⁵ T. -M. Chuang, M. P. Allan, J. Lee, Y. Xie, N. Ni, S. L. Bud'ko, G. S. Boebinger, P. C. Canfield, and J. C. Davis, *Science*, **327**, 181 (2010).
 - ³⁶ C. Fang, H. Yao, W. F. Tsai, J. P. Hu, and S. A. Kivelson, *Phys. Rev. B* **77**, 224509 (2008).
 - ³⁷ Y. Qi and C. Xu, *Phys. Rev. B* **80**, 094402 (2009).